**Molecular Cell, Volume *71***

## Supplemental Information

# Reconstitution of a 26-Subunit Human Kinetochore Reveals Cooperative Microtubule Binding by CENP-OPQUR and NDC80

**Marion E. Pesenti, Daniel Prumbaum, Philip Auckland, Charlotte M. Smith, Alex C. Faesen, Arsen Petrovic, Muriel Erent, Stefano Maffini, Satyakrishna Pentakota, John R. Weir, Yu-Chih Lin, Stefan Raunser, Andrew D. McAinsh, and Andrea Musacchio**

**Supplementary material for**

# Reconstitution of a 26-subunit human kinetochore reveals cooperative microtubule binding by CENP-OPQUR and NDC80

by Marion E. Pesenti *et al.*

Including

Supplemental Figures S1 to S7, Table S1, and Movie S1, and their legends

**Figure S1. Reconstitution and characterization of the human CENP-OPQUR complex; Related to Figure 1**

**A-B**) Elution profiles and corresponding SDS-PAGE of recombinant CENP-OP and CENP-QU complexes. **C**) Elution profiles and SDS-PAGE analysis of a stoichiometric mixture of CENP-OP (blue) and CENP-QU (red) resulting in the formation of the four subunits complex CENP-OPQU (black). **D**) Elution profiles and corresponding SDS-PAGE of recombinant CENP-OPQU obtained by co-expression. **E**) Sedimentation velocity AUC demonstrated that each CENP-OPQUR complex and sub-complexes contained single copies of each subunit. CENP-R when expressed in isolation forms a tetramer. **F**) Elution profile and corresponding SDS-PAGE of recombinant CENP-R. **I**) Elution profile and corresponding SDS-PAGE of recombinant CENP-OPQUR obtained by co-expression in insect cells. **G-H**) Elution profiles and SDS-PAGE analysis of stoichiometric mixtures of CENP-R and CENP-OP (in G) or CENP-QU (in H). No strong direct interaction of isolated CENP-R with either CENP-OP or CENP-QU was observed. Note that the gel illustrating the elution of CENP-R (middle) in panels G and H has been intentionally duplicated to visualize elution shifts (or lack thereof). **J**) Insect cell co-expression of CENP-R with CENP-OPQU (positive control) or CENP-QU results in the identification of CENP-R in the elution fraction after purification with His-CENP-PO and/or His-CENP-QU. When co-expressed, CENP-R does not bind CENP-OP. Thus, CENP-R interacts predominantly with CENP-QU subunit. (T, Total cleared lysate; SN, Soluble faction; FT, Flow Through; E, Elution). **K**) Representative images show the localization of recombinant CENP-OPQUR labeled with Alexa488 (green) in mitotic cells after electroporation into interphase cells. CREST syndrome autoantibodies identify kinetochores. Scale bar = 5 μm. **L**) Elution profiles and SDS-PAGE analysis of a stoichiometric mixture of CENP-OP (blue) and CENP-$Q^{68\text{-}C}$U (red) resulting in the formation of the four subunits complex CENP-OP$Q^{68\text{-}C}$U (black).

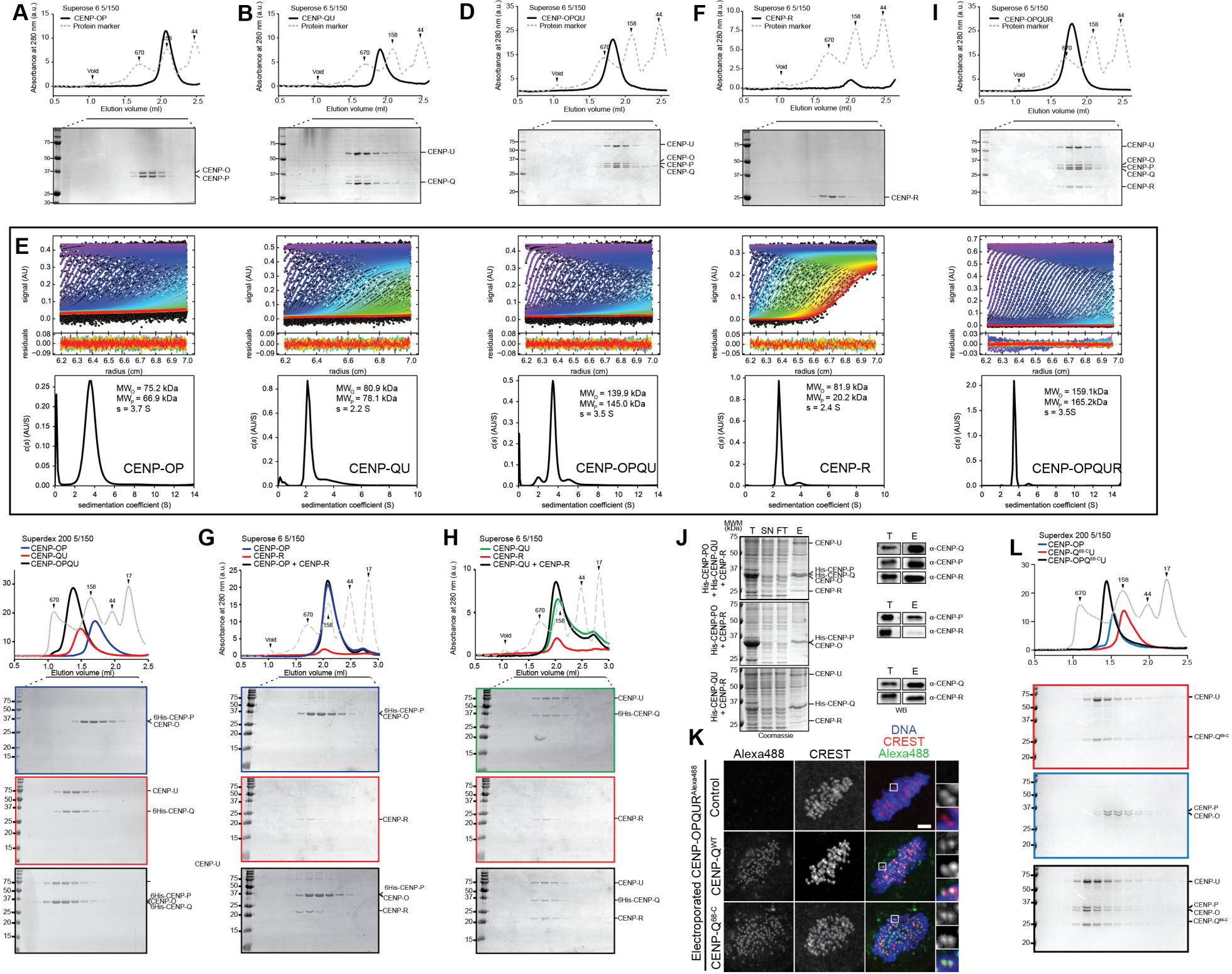


Pesenti et al. Figure S1

**Figure S2. Localization dependencies; Related to Figure 2**

**A**) Western blot showing the depletion of CENP-H in each of the GFP-CENP-OPQUR HeLa FlpIn TRex stable cell lines. **B**-**E**) Representative images of HeLa FlpIn TRex cells stably expressing GFP-CENP-O (B), GFP-CENP-P (C), GFP-CENP-R (D), and GFP-CENP-U (E), where CENP-H, CENP-L, and CENP-N have been depleted by RNAi. CENP-O, -P, -U, and –R are all lost from the kinetochore in the absence of CENP-H, -L, or –N. The CENP-HK complex is also lost from kinetochores during the aforementioned RNAi depletions. Quantification of the GFP-CENP-OPUR proteins after the indicated depletion are shown to the right of their respective images in green, CENP-HK is shown in red. **$p \leq 0.01$. Graph shows results from one of three independent experiments, a minimum of 158 (CENP-O), 113 (CENP-P), 54 (CENP-U), or 124 (CENP-R) kinetochores were quantified for the cell line indicated in brackets. All scale bars = 5 μm. **F**) Assessment of depletion levels for the RNAi experiments. Western blot showing the depletion of CENP-O, -P, -Q, or –R from FlpIn TRex cells stabling expressing GFP-CENP-R. **G**) Co-localization studies were carried out by depleting CENP-O, CENP-P, CENP-Q, or CENP-R, using RNAi, from HeLa FlpIn TRex cells stabling expressing GFP-CENP-R. Cells were stained with antibodies targeting CENP-OP, CENP-QU, and Nsl1. Insets identify kinetochores. Scale bar = 5 μm. **H**) Quantification of the co-localization of CENP-OP, CENP-QU, and GFP-CENP-R following depletion of CENP-O, CENP-P, CENP-Q, and CENP-R in HeLa FlpIn TRex cells. The graph shows a minimum of 276 kinetochores from at least three technical replicas of the experiment. **I**) Mitotic index of cells depleted of CENP-O, CENP-P, CENP-Q, CENP-R, or left untreated. Depletion of any CENP-O complex protein significantly increased the mitotic index as compared to the untreated control, indicating that CENP-OPQUR has a role in mitotic progression. **$p \leq 0.01$.

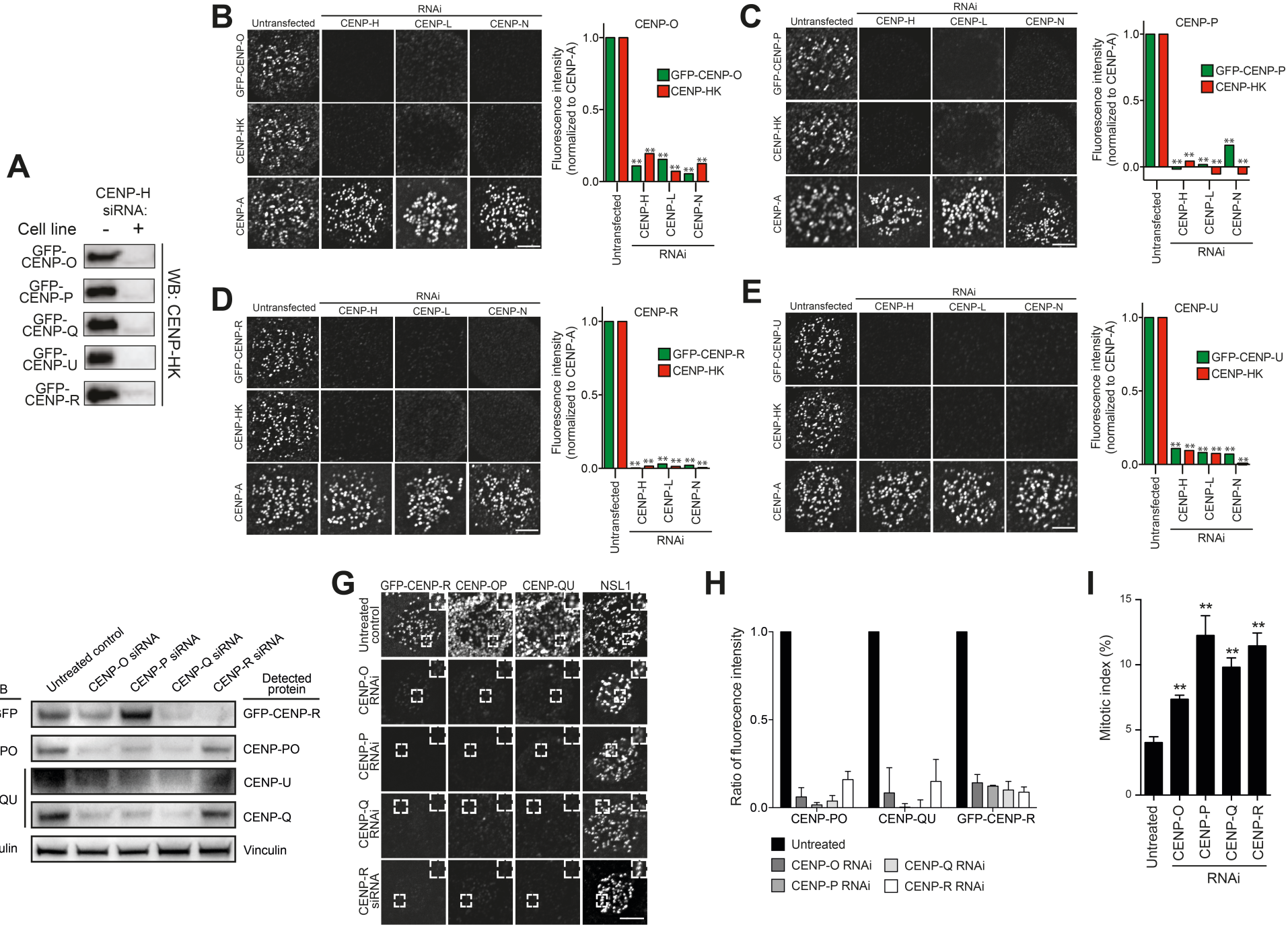


Pesenti et al Figure S2

**Figure S3. RWD domains in CENP-OP and Knl1 have similar interaction modes with their targets; Related to Figure 2**

**A-C**) Elution profiles and subsequent SDS-PAGE of the recombinant CENP-$C^{1-544}$, CENP-HIKM, and CENP-LN complexes. **D-E**) Cartoon models comparing the RWD domains of Knl1 (residues 2106-2311; PDB access number 4NF9) and Ctf19 (residues 96–269; PDB access number 3ZXU). Tyr2125 of Knl1 is the residue responsible for the binding of Nsl1. Phe138 of Ctf19 (F116 in human CENP-P) is conserved and its position it close related to that of Knl1 Tyr2125. **F**) Sequence alignment of CENP-P and Ctf19 from the indicated species in the region containing Phe116. **G**) Pull-down assays using SNAP-CENP-$C^{1-544}$ bait. CENP-$OP^{F116G}$ (2 μM) fails to bind to immobilized CENP-CHIKMLN, and further prevents binding of CENP-QU (also at 2 μM). The experiment shown is representative of at least 3 repeats. **H**) Immunoprecipitation (IP) assays were carried out using cell lines that stably expressed GFP-CENP-P or its respective RWD domain mutants GFP-CENP-$P^{F116G}$. The mutation of the CENP-P RWD domain disrupted its interaction with CENP-HK and CENP-QU, while maintaining its binding to CENP-N. Lysates from cells expressing GFP alone where used as a control and did not interact with any of the aforementioned proteins.

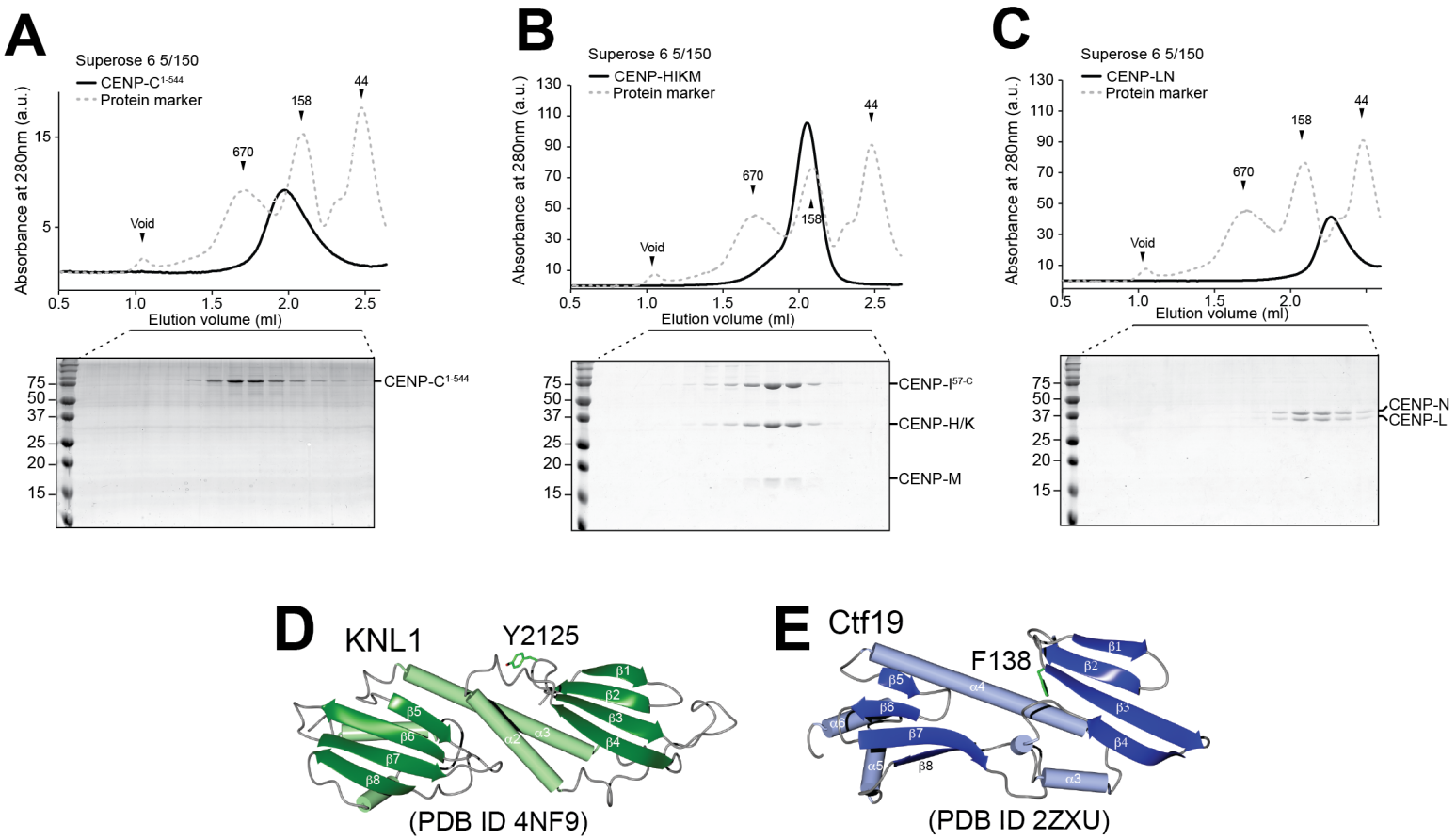








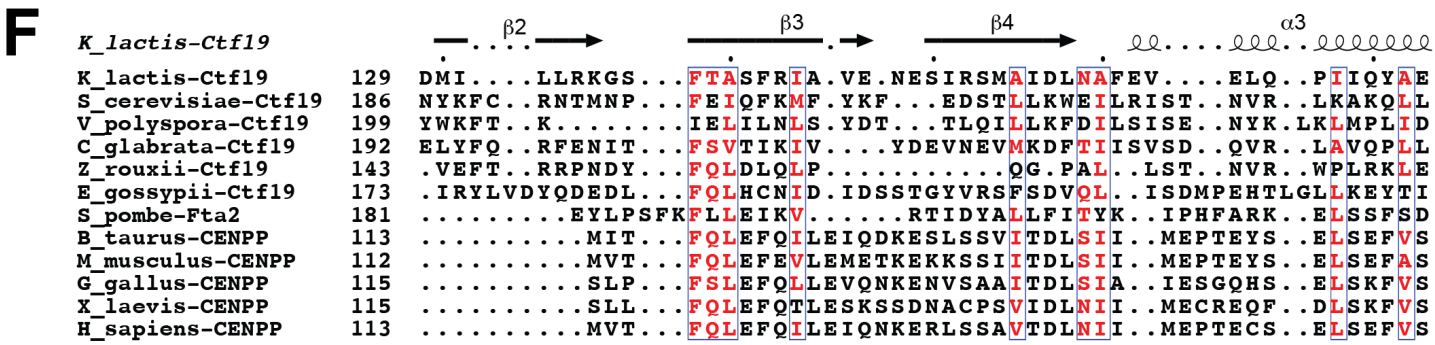


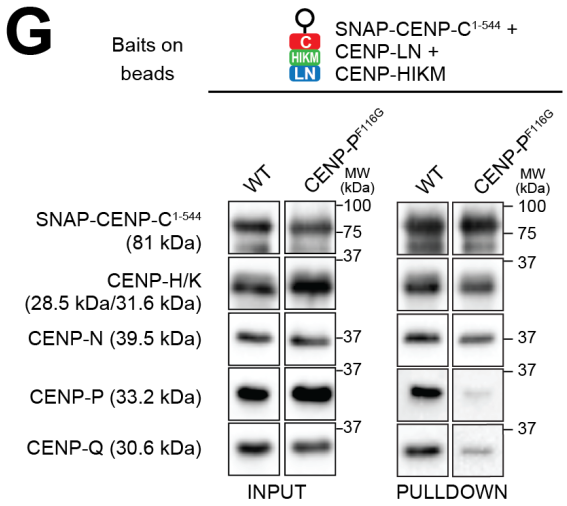


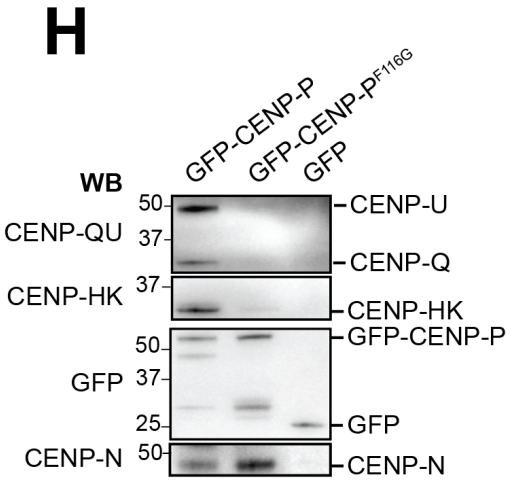


Pesenti et al
Figure S3

**Figure S4. Analytical SEC and SDS-PAGE analysis of stoichiometric mixtures of CENP-OPQUR with different kinetochore subunits; Related to Figures 3 and 6**

**A-B**) The omission of CENP-LN or CENP-HIKM prevents the interaction of CENP-OPQUR with CENP-HIKM and CENP-LN, respectively. **C-F**) CENP-OPQUR cannot form a complex with any other KT subunits if it is not incorporated in the CENP-HIKMLNOPQUR complex. Note that the gels illustrating the elution of CENP-OPQUR in panels A-B, C-D, or E-F have been intentionally duplicated to visualize elution shifts (or lack thereof) when mixing with potential binding partners. The same is true of the gel illustrating the elution of the mixture containing CENP-OPQUR, CENP-$C^{1\text{-}544}$, MIS12C, and NDC80C, which was intentionally duplicated in panels E-F (bottom).

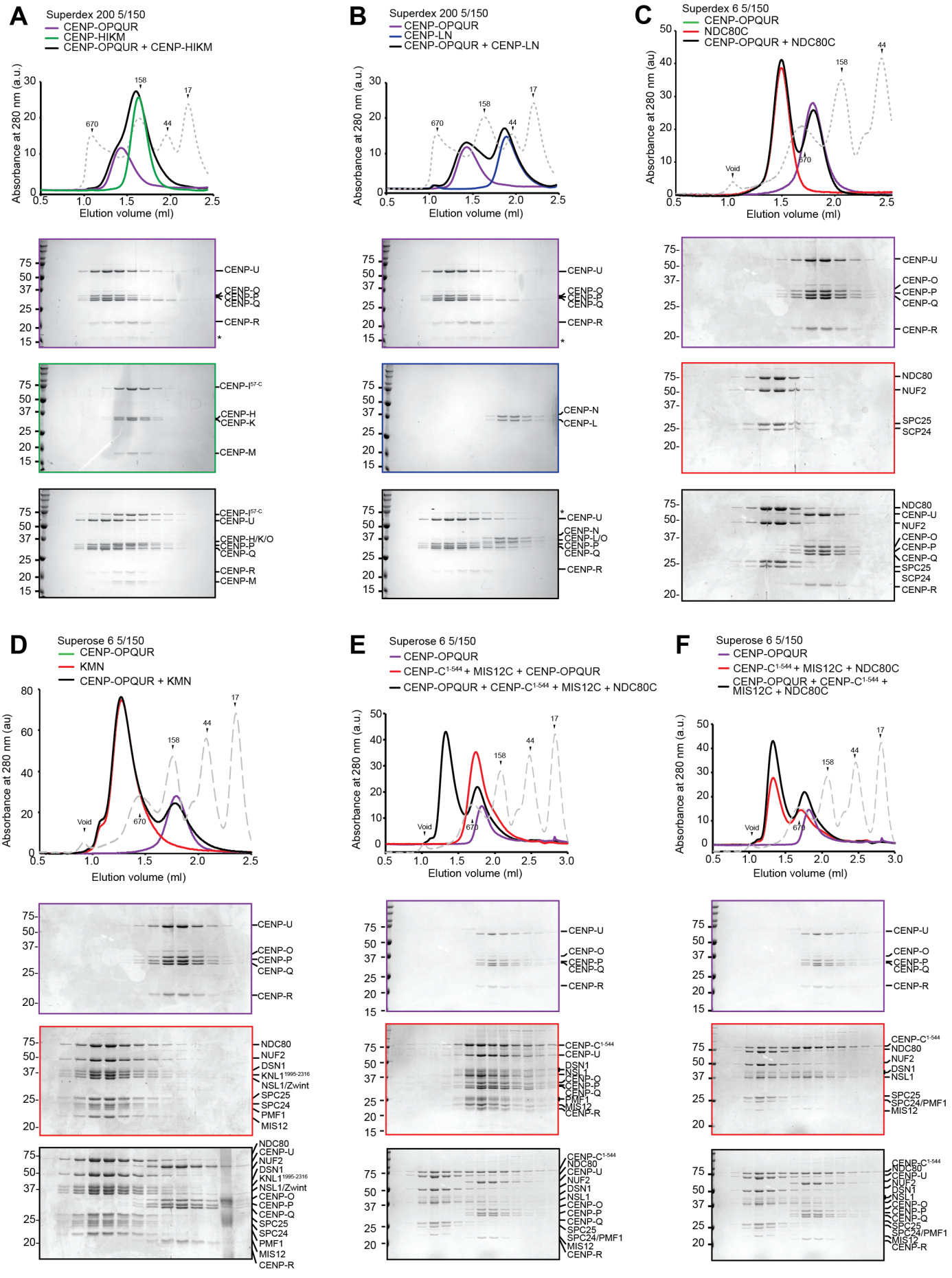


Pesenti et al Figure S4

**Figure S5. CENP-HIKMLNOPQUR complex and the rKT26. Related to Figures 3 and 4.**

**A)** Primary data and fitting residuals for the AUC run in Figure 3C. **B-C**) SDS-PAGE analysis of the fractions collected after GraFix procedure of the CENP-HIKMLNOPQUR complex in absence (A) and presence (B) of glutaraldehyde (Kastner et al., 2008). In fraction 12, all the 11 proteins are presents (A) and form a slow migrating band when cross-linked (B). **D**) Fraction 12 of the cross-linked sample was analyzed by Western blotting and shown to contain the 11 subunits. **E-F**) Electron densities of CENP-HIKM (green) and CENP-OPQUR (violet) were manually fitted into CENP-HIKMLNOPQUR. Inspection of the volume reveals that the sub-complexes do not occupy the full volume, leaving additional space that was attributed to the LN sub-complex (see also Figure 3E-H). The difference map was created using Chimera and filtered to 20 Å resolution. For an additional visualization see Movie 1. Scale bar = 10 nm. **G-J**) Elution profiles and SDS-PAGE of recombinant subunits of human kinetochore proteins used for the assembly of the rKT26. Every subunit or complex elutes in a single peak with a retention volume larger than that of rKT26.

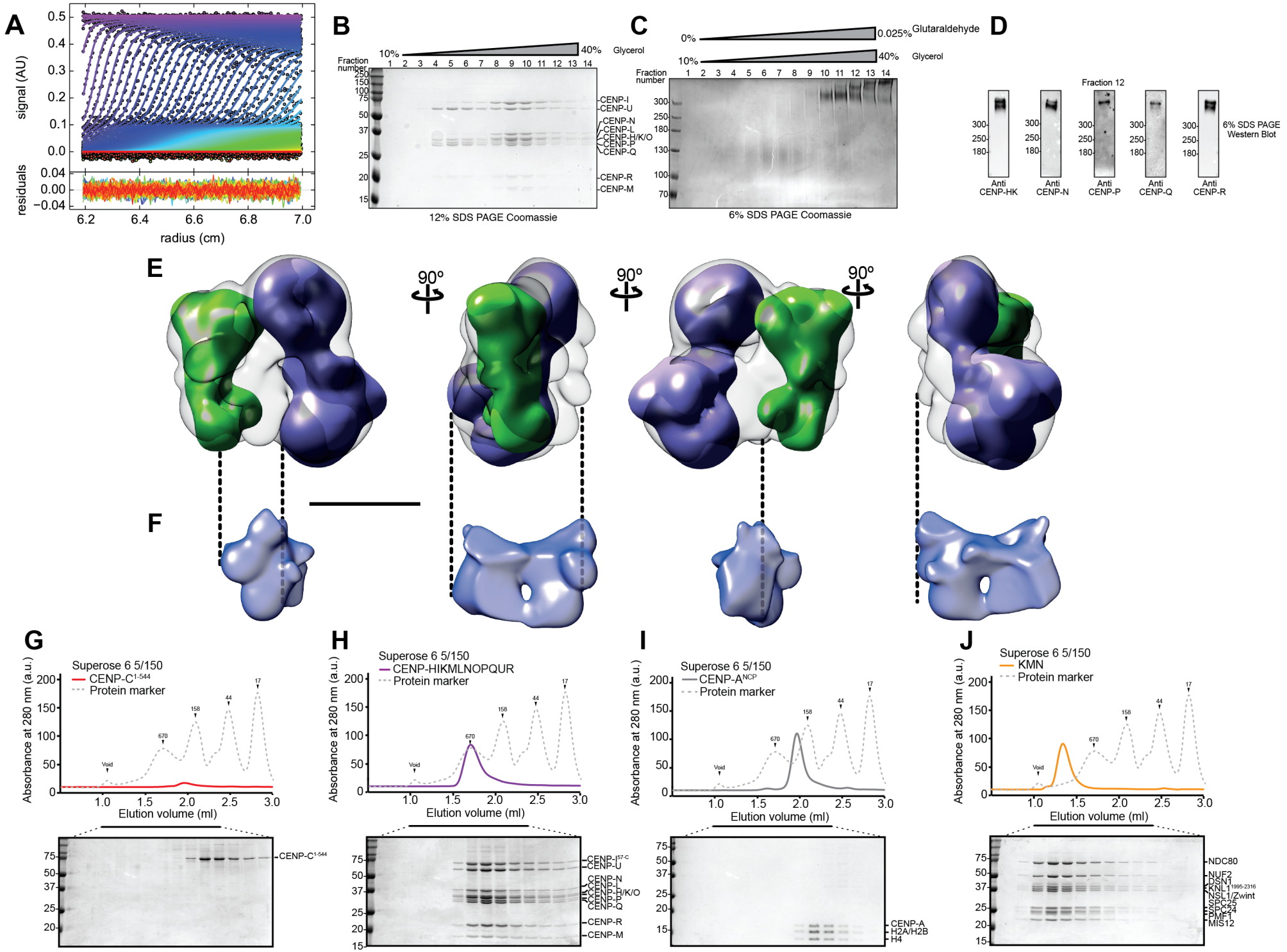


Pesenti et al Figure S5

**Figure S6. CENP-OPQUR complex binds microtubules via CENP-QU and CENP-R subunits; Related to Figures 3 and 5**

**A**) Representative electron micrograph area of the negatively stained CENP-OPQU complex. Scale bar = 100 nm (10 nm, enlarged). The resolution was estimated by the Fourier shell correlation (FSC) 0.5 criterion to be ~23 Å. A Collection of class averages of the CENP-OPQU complex derived from a data set of 4745 single particles. Selected Reprojections of the 3D reconstruction paired with their corresponding class averages. Scale bar = 10 nm. **B**) Representative electron micrograph area of the negatively stained CENP-OPQUR complex. Scale bar = 10 nm. The resolution was estimated by the Fourier shell correlation (FSC) 0.5 criterion to be ~23 Å. A Collection of class averages of the CENP-OPQUR complex derived from a data set of 3260 single particles. Selected Reprojections of the 3D reconstruction paired with their corresponding class averages. Scale bar = 10 nm. **C**) Representative SDS-PAGE of microtubule co-sedimentation assays of 1 μM CENP-OP, CENP-QU, CENP-R, CENP-OPQU, CENP-OPQUR, CENP-OPQ$^{68\text{-}C}$U, and CENP-OPQ$^{68\text{-}C}$UR with 10 μM taxol-stabilized microtubules. P, pellet fraction; S, soluble fraction. A subset of panels from this figure are additionally shown in Figure 5A. **D**) Quantification of experiments in **C**. Error bars are standard deviations calculated from three technical replicas. **E**) Representative electron micrographs of negatively stained microtubules bundled upon exposure to increasing concentration of CENP-OPQU complex. Scale bar = 40 nm. **F**) Additional representatives electron micrographs of negative-stained Taxol-stabilized microtubules in presence of CENP-OPQUR. The outline of the complex, recognizable on the microtubule surface, suggests that the microtubule-binding moiety is in the base domain. Scale bar = 20 nm. **G**) Representative electron micrograph area of the negatively stained CENP-HIKMLNOPQUR complex. A Collection of selected reprojections of the 3D reconstruction of the CENP-HIKMLNOPQUR complex paired with their corresponding class averages derived from a data set of 10515 single particles. Scale bar = 20 nm. The resolution was estimated by the Fourier shell correlation (FSC) 0.5 criterion to be ~22 Å.

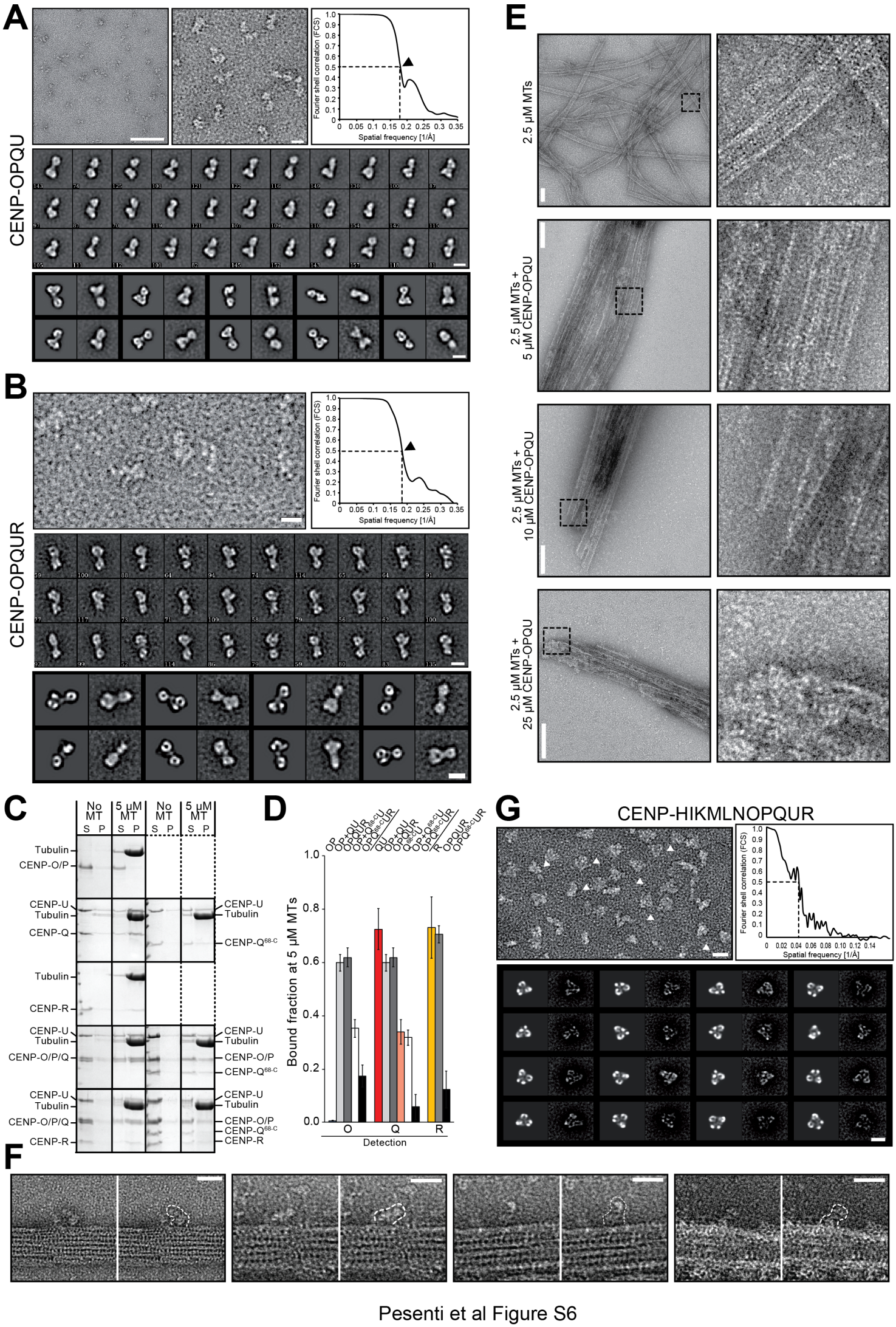


Pesenti et al Figure S6

**Figure S7. SEC analysis demonstrating interaction of CENP-OPQ$^{68\text{-}C}$UR mutant with rKT21 and various alignment and checkpoint assays; Related to Figures 6 and 7**

**A**) Analytical SEC and SDS-PAGE analysis of stoichiometric mixtures of CENP-OPQ$^{68\text{-}C}$UR with CENP-11 subunits demonstrating complex assembly. In panels B-D, we demonstrate that depletion of CENP-OPQUR subunits is associated with a variety of spindle assembly and chromosome alignment problems, with delayed mitotic exit and frequent lagging chromosomes at anaphase, phenotypes that are strongly exacerbated during recovery from spindle damage (Bancroft et al., 2015; Hori et al., 2008b; Hua et al., 2011; McAinsh et al., 2006; McClelland et al., 2007; Minoshima et al., 2005; Toso et al., 2009). For reasons that remain unclear, penetrance of these effects varies considerably in different cell and organismal models (Kagawa et al., 2014; McKinley et al., 2015). After depleting CENP-P by RNAi, we monitored the timing of mitotic progression by time-lapse video microscopy in HeLa cells. We show that addition of Reversine, an inhibitor of the spindle assembly checkpoint kinase Mps1 (Santaguida et al., 2010), promoted very rapid anaphase in CENP-P depleted cells, indicating that the mitotic delay is caused by checkpoint activation (panel B). In an established chromosome bi-orientation assay, in which HeLa cells were first treated with STLC (an inhibitor of the Eg5 kinesin) to prevent spindle bipolarization, and then allowed to bipolarize by STLC washout before fixation, CENP-P-depleted cells contained a high proportion of chromosomes that had failed to bi-orient, indicating that the CENP-OPQUR contributes to chromosome bi-orientation (panel C). Finally, the chromosome alignment defects caused by depletion of CENP-P and CENP-Q were at least partially rescued after electroporation of recombinant CENP-OPQUR complex, but not of CENP-OPQ$^{68\text{-}C}$UR complex (panel D). **B**) Additional immunofluorescence images of the tail-swap rescue experiment described and quantified in Figure 7B-E. Here, we chose two cells in the same field of view that had either received (cell 1) or not received (cell 2) the CENP-Q-eGFP rescue construct. Note kinetochore localization of CENP-E in cells expressing CENP-Q-eGFP and lack thereof in non-transfected cells. Scale bar 5 μm. **C**) As in B, but showing a field of view from cells that had (cell 1) or had not (cell 2) received the CENP-Q$^{NDC80(1\text{-}80)}$-eGFP transgene. **D**) The CENP-OPQUR complex is required for recovery from nocodazole. Quantification of time-lapse microscopy experiments on U2OS cells, either untreated, depleted of CENP-P, or depleted of CENP-P and treated with 0.5 μM

Reversine, progressing to anaphase after release (time 0) from a 16-hour nocodazole (330 nM) treatment. **E**) Recovery from monopolarity is impaired in absence of the CENP-OPQUR complex. Quantification of experiments in which U2OS cells were synchronized for 16 hours with 5 μM STLC, an Eg5 inhibitor, then released in inhibitor-free medium containing MG132 and fixed after 3 h. Loss of the CENP-OPQUR complex resulted in a large fraction of cells with misaligned chromosomes, indicative of error correction problems. **F**) Cells depleted for CENP-Q/P and electroporated either with Alexa-488 labeled CENP-OPQ$^{WT}$UR or CENP-OPQ$^{68\text{-}C}$UR. Following synchronisation with STLC treatment, cells were released MG132 containing medium for 150 minutes before being prepared for immunofluorescence analysis and scored for the presence of uncongressed chromosomes. When compared with CENP-OPQ$^{WT}$UR, electroporation of CENP-OPQ$^{68\text{-}C}$UR results in a larger fraction of cells with uncongressed chromosomes.

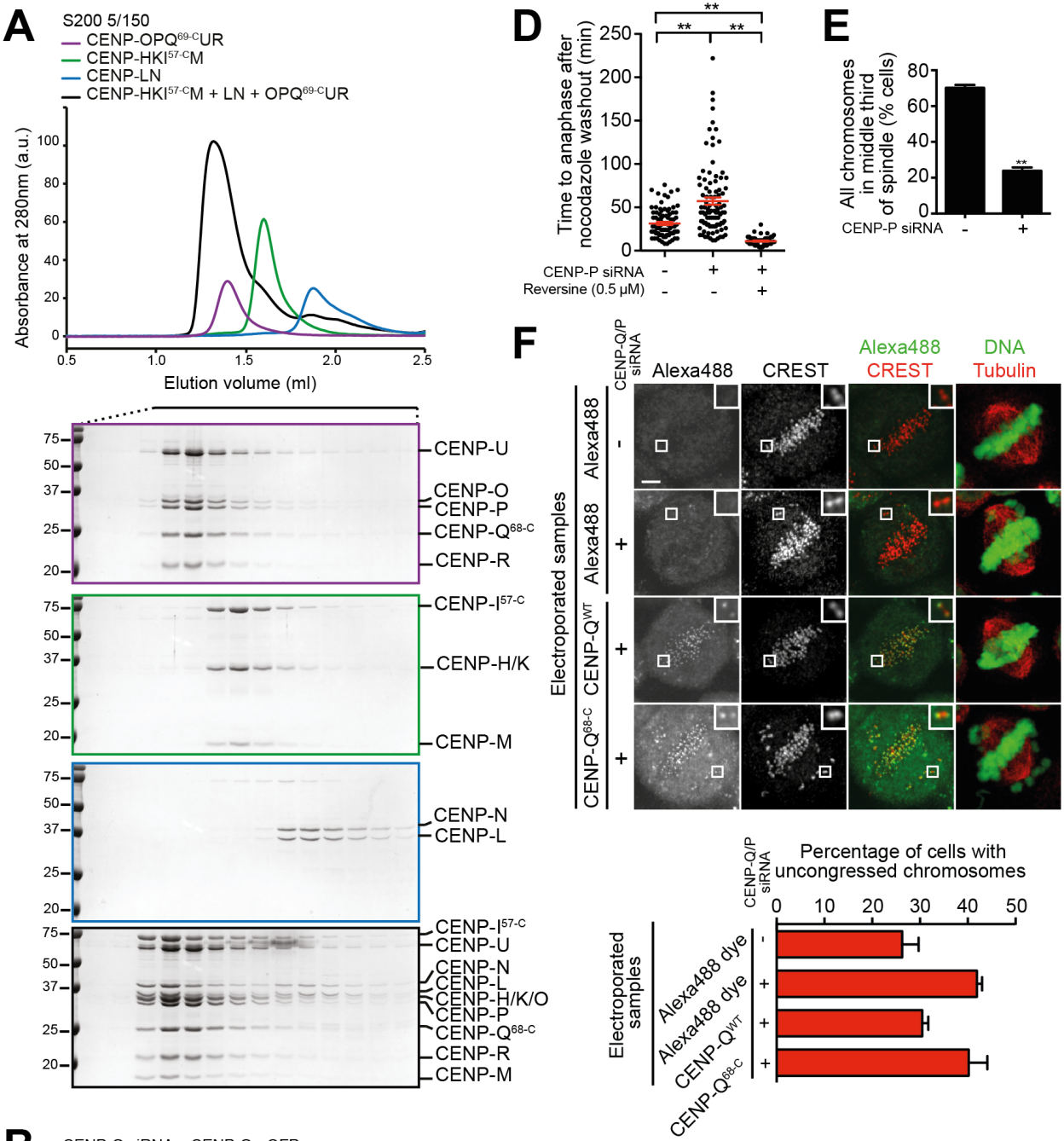


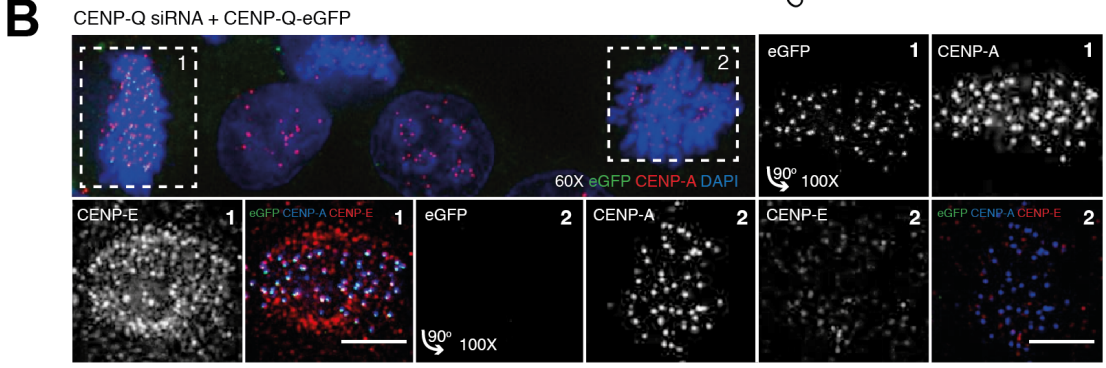


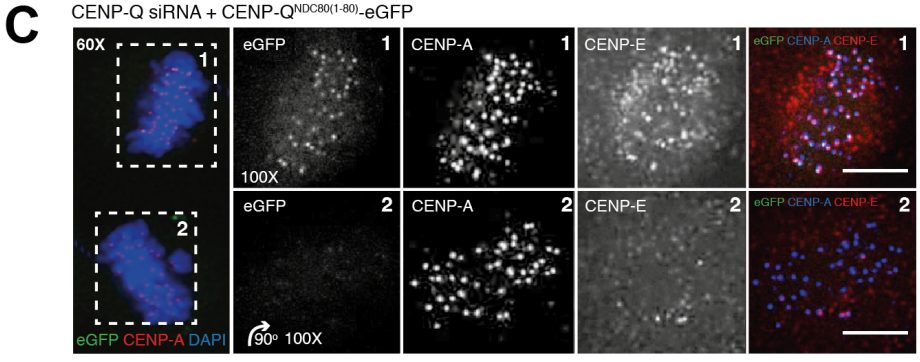


Pesenti et al Figure S7

**Table S1. Sedimentation velocity analytical ultracentrifugation (AUC) of indicated kinetochore complexes; Related to Figure 3**

**Table S1**

*Sedimentation velocity analytical ultracentrifugation (AUC) of indicated kinetochore complexes*

| Experiment | Complex | Predicted mass (kDa) | Observed mass (kDa) | Frictional ratio | Sedimentation coefficient (S) | Predicted stoichiometry |
|---|---|---|---|---|---|---|
| 1 | CENP-OP | 66.9 | 75.2 | 1.3 | 3.7 | 1:1 |
| 2 | CENP-QU | 78.1 | 80.9 | 2.3 | 2.2 | 1:1 |
| 3 | CENP-R | 20.2 | 81.9 | 2.2 | 2.5 | Tetramer |
| 4 | CENP-OPQU | 145.0 | 139.9 | 1.8 | 3.5 | 1:1:1:1 |
| 5 | CENP-OPQUR | 165.2 | 159.1 | 2.2 | 3.5 | 1:1:1:1:1 |
| 6 | CENP-HIKMLNOPQUR | 404.0 | 407.7 | 1.7 | 7.7 | 1:1:1:1:1:1:1:1:1:1:1 |